Int J Fract (2020) 224:253–260
https://doi.org/10.1007/s10704-020-00451-5

BRIEF NOTE

Hydrogen embrittlement resistance of pre-strained ultra-high-strength low alloy TRIP-aided steel

Tomohiko Hojo · Bakuya Kumai · Motomichi Koyama · Eiji Akiyama · Hiroyuki Waki · Hiroyuki Saitoh · Ayumi Shiro · Ryo Yasuda · Takahisa Shobu · Akihiko Nagasaka

Received: 3 December 2019 / Accepted: 27 April 2020 / Published online: 8 June 2020

Abstract In the study, the pre-strain effect on hydrogen embrittlement property of the ultra-high-strength transformation-induced plasticity (TRIP)-aided bainitic ferrite (TBF) steel was investigated towards application for automobile frame parts. Specifically, 3–10% tensile pre-strain suppressed hydrogen-induced mechanical degradation relative to total elongation (pre-strain + elongation after hydrogen charging) while 12–15% pre-strained specimen did not exhibit elongation after hydrogen charging. The advantageous effect of the 3–10% pre-strain was attributed to the suppression of crack initiation related to retained austenite. Specifically, the TRIP by pre-straining decreased the volume fraction of retained austenite before hydrogen charging, thereby reducing existing probabilities of preferential crack initiation sites and propagation paths. Conversely, high pre-strain such as 12–15% does not effectively work due to work hardening resulting in increases in hydrogen embrittlement susceptibility and a significant increase in hydrogen content due to the multiplication of dislocations.

Keywords TRIP-aided steel · High-strength steels · Hydrogen embrittlement · Retained austenite · Pre-strain

T. Hojo (✉) · B. Kumai · M. Koyama · E. Akiyama
Institute for Materials Research, Tohoku University, 2-1-1 Katahira, Aoba-ku, Sendai, Miyagi 980-8577, Japan
e-mail: hojo@imr.tohoku.ac.jp

B. Kumai
Graduate Student, Tohoku University, 6-6 Aoba, Aramaki-ji, Aoba-ku, Sendai, Miyagi 980-8579, Japan

H. Waki
Faculty of Science and Engineering, Iwate University, 4-3-5 Ueda, Morioka, Iwate 020-8551, Japan

H. Saitoh · A. Shiro · R. Yasuda
National Institutes for Quantum and Radiological Science and Technology (QST), 1-1-1 Kouto, Sayo, Hyogo 679-5148, Japan

T. Shobu
Japan Atomic Energy Agency (JAEA), 1-1-1 Kouto, Sayo, Hyogo 679-5148, Japan

A. Nagasaka
Department of Mechanical Engineering, National Institute of Technology, Nagano College, 716 Tokuma, Nagano 381-8550, Japan

1 Introduction

High-strength steel sheets of 780-MPa- and 980-MPa-grade are used for automobile frame parts to secure crash safety of passengers and improve fuel efficiency because they decrease the body weight of vehicles. Furthermore, 1470-MPa-grade ultra-high-strength steel sheets that are produced via hot stamping technique (Senuma and Takemoto 2010; Zhou et al. 2014) are used for the frame parts of vehicles. Conversely, 780-MPa- and 980-MPa-grade high-strength steel sheets are typically processed by cold stamping. It is widely known that press formabilities deteriorate when tensile strength of conventional high-strength steel sheets exceeds 980 MPa, which has been regarded as a prob-

lem in cold stamping. It is also known that hydrogen embrittlement is a serious problem in ultra-high-strength steel sheets with tensile strength over 980 MPa. Thus, hydrogen embrittlement resistance of ultra-high-strength steel sheets have been investigated (Takagi et al. 2012, 2016).

From the formability viewpoint, the use of transformation-induced plasticity (TRIP) (Zackay et al. 1967) is a pathway to solve the problem in cold stamping. For example, TRIP-aided bainitic ferrite (TBF) (Caballero et al. 2008, 2013; Hojo et al. 2008, 2016, 2017, 2018; Peet and Hojo 2016; Song et al. 2003; Sugimoto et al. 2002, 2004; Yoshikawa et al. 2012), for which the matrix is bainitic ferrite, is expected to be used as the cold stamping ultra-high-strength steel with tensile strength of over 980 MPa because the TBF steel exhibits excellent press formabilities (Caballero et al. 2008; Sugimoto et al. 2002, 2004), impact property (Caballero et al. 2013; Hojo et al. 2016), and fatigue property (Song et al. 2003; Yoshikawa et al. 2012) associated with the TRIP of retained austenite. Furthermore, superior hydrogen embrittlement resistance (Hojo et al. 2008, 2017, 2018; Peet and Hojo 2016) is also reported due to the high hydrogen absorption capacity of retained austenite. Therefore, hydrogen embrittlement properties of the TBF steel attracted attention in terms of exploring practically available high-performance high-strength steels.

Understanding pre-strain effect before hydrogen uptake is a key to simulate the press forming and cold stamping for automobile parts. However, there is a paucity of investigations of hydrogen embrittlement property of pre-strained TBF steels. In the study, the effect of pre-straining on hydrogen embrittlement resistance of a TBF steel was investigated towards application as cold stamping ultra-high-strength steel sheets.

2 Experimental procedure

Cold-rolled steel sheet with a chemical composition of 0.4C-0.49Si-1.51Mn-1.02Al-0.05Nb-0.2Mo-0.0015O-0.0019N (mass %) was used in the study. The martensite-transformation-start-temperature (M_S) (Tamura 1970) was estimated as 376 °C. The cold-rolled steel sheet was annealed at 915 °C for 1200 s followed by austempering treatment at 425 °C for 500 s to obtain bainitic ferrite matrix with an approximately 10% interlath and blocky retained austenite as shown in Fig. 1. The carbon content in the retained austenite was estimated as 1.20 mass% from a lattice constant (Dyson and Holmes 1970).

Variation in the volume fraction of retained austenite during tensile testing was measured via the energy dispersion method using synchrotron white X-rays and Ge semiconductor detector at BL14B1 in SPring-8. The X-rays were shaped with a height of 50 μm and a width of 300 μm via slits set at an incident side, and X-rays penetrated through the sample were limited by a collimator of 50–200 μm with a 500-μm slit. The diffraction angle of the detector was set at 10°. From the energy spectrum obtained by the X-ray diffraction analysis, the peaks corresponding to 200_α, 211_α, 220_α, 200_γ, 220_γ and 311_γ were approximated using a Gaussian function, and an integrated intensity was obtained from Gaussian curve fit to those peaks. The volume fraction of retained austenite was estimated by the average of ratio of the integrated intensities of α and γ peaks. A tensile test of the specimen shown in Fig. 2 was performed at a crosshead speed of 0.03 mm/min using a home-made small tensile testing machine.

Additionally, dislocation patterns were observed via transmission electron microscopy (TEM) at an acceleration voltage of 200 kV. The specimens for TEM were prepared by the Ion Slicer (EM-09100IS produced by JEOL). Fracture surface and specimen surface were observed via scanning electron microscopy at an acceleration voltage of 15 kV.

Tensile pre-straining was applied to an as-heat-treated specimen with dimensions of 50 mm in gauge length, 12.5 mm in width, and 1.2 mm in thickness at a crosshead speed of 1 mm/min at 25 °C. Subsequently, specimens with different pre-strains were charged with hydrogen. Tensile tests were performed at the same tensile test condition as pre-straining. Hydrogen embrittlement property was evaluated by total elongation, TEl_f. Total elongation in the study is defined as follows:

$$TEl_f = \varepsilon_{pre} + \varepsilon_m \quad (1)$$

where ε_{pre} and ε_m denote elongations during pre-straining and after hydrogen charging, respectively.

Hydrogen was introduced via a cathode charging method using a 3 wt% NaCl and 3 g/L NH_4SCN aqueous solution at current densities corresponding to 1 and 10 A/m^2 at 25 °C for 48 h. A platinum wire was used as an anode. Hydrogen concentration (mass ppm, hereafter ppm) was measured via thermal desorption spectrometry (TDS) using quadrupole mass spectrometry.

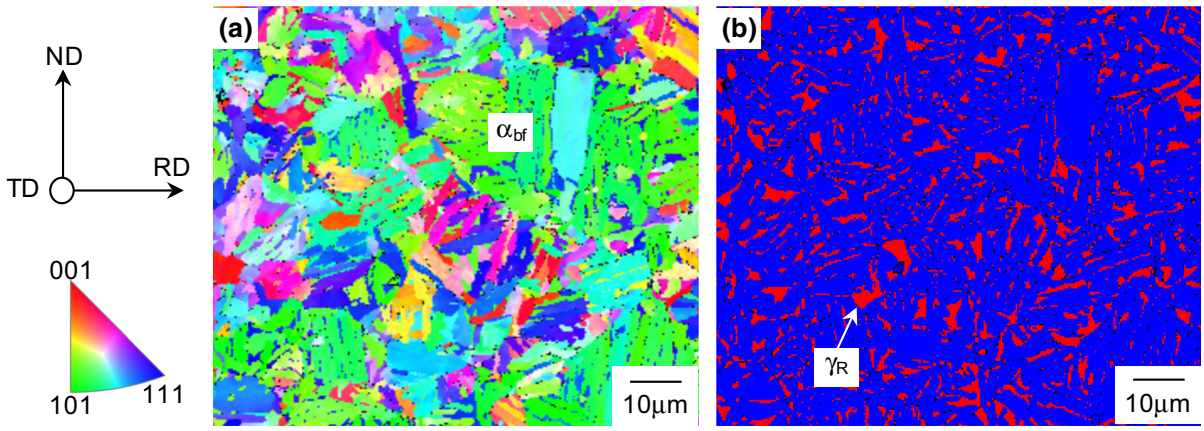

Fig. 1 **a** Inverse pole figure (IPF) of RD direction and **b** phase maps of the as-heat-treated TBF steel. α_{bf} in (**a**) and γ_R in (**b**) denote bainitic ferrite and retained austenite, respectively. The electron backscatter diffraction measurement is performed at a beam step size of 0.17 nm. Specifically, RD, TD, and ND represent rolling, transverse, and normal directions, respectively. Red and blue regions in (**b**) represent fcc (retained austenite) and bcc (bainitic ferrite) phases, respectively

The TDS measurements were conducted after tensile testing. Specimens were heated from room temperature to 800 °C at a heating rate of 100 °C/h. Diffusible hydrogen was defined as hydrogen desorbed below 300 °C. Specimens after the tensile tests were placed in liquid nitrogen to prevent hydrogen desorption prior to TDS measurements.

The average size of retained austenite was defined as diameters for blocky retained austenite and length for filmy retained austenite, which were measured from phase map obtained by an electron backscatter diffraction measurement with a beam step size of 170 nm at an acceleration voltage of 15 kV. On the other hand, the dimple size was defined as average length of major and minor axes after elliptic approximation of its shape, which was measured from scanning electron micrographs of fracture surfaces.

3 Results and discussion

3.1 Microstructure and tensile properties

First, we present basic mechanical and microstructural characteristics of the present TBF steel without hydrogen charging. Table 1 lists the tensile properties and retained austenite characteristics of the as-heat-treated TBF steel. Figure 2 shows the transformation behavior of retained austenite during tensile testing. The volume fraction of retained austenite decreased with increases in the plastic strain. Approximately, 4 vol% austenite still remained even after 23% plastic straining that corresponded to uniform elongation. The same experiment was carried out for another specimen, and we confirmed the reproducibility of the changing trend of austenite fraction with strain. Simultaneously, dislocation density increases with increases in the strain as shown in Fig. 3.

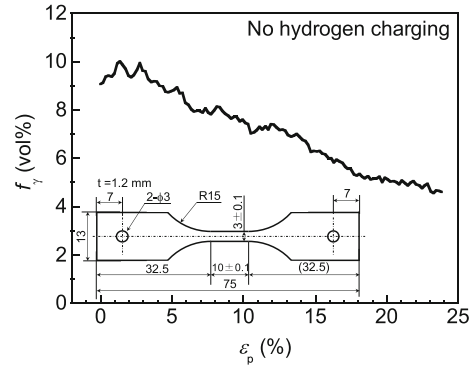

Fig. 2 Variation in volume fraction of retained austenite (f_γ) as a function of plastic strain (ε_p)

3.2 Hydrogen embrittlement properties

Figure 4 shows nominal stress–strain curves of the TBF steel after pre-straining to 0, 6, and 12% with hydrogen charging at current densities corresponding to 1 and

Table 1 Tensile properties and retained austenite characteristics of TBF steel

Tensile strength	0.2% proof stress	Uniform elongation	Total elongation	Initial volume fraction of retained austenite	Initial carbon concentration of retained austenite
996 MPa	831 MPa	23%	29%	9.9 vol%	1.20 mass%

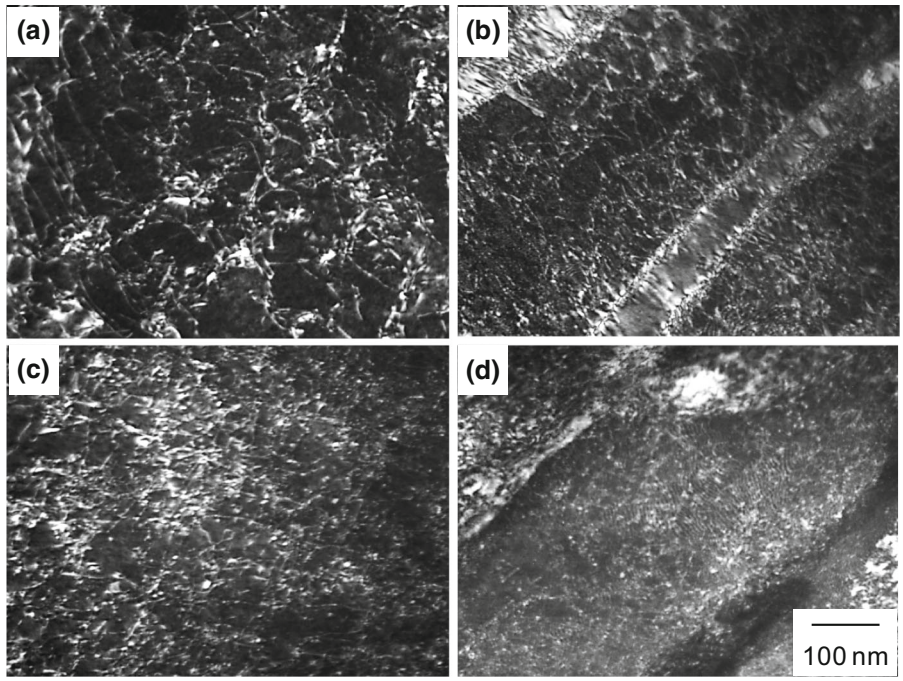

Fig. 3 TEM micrographs of dark field image of specimens strained to **a** 0%, **b** 6%, **c** 10%, and **d** 15% without hydrogen charging

10 A/m^2. The dotted lines denote nominal stress–strain curves without pre-straining and hydrogen charging. The hydrogen charging significantly decreased fracture strain. When the pre-strain was 12%, plastic deformation barely occurred in the hydrogen charged specimen. The diffusible hydrogen contents after fracture as measured by TDS are also shown in Fig. 4.

Figure 5 shows total elongation (TEl_f) as a function of pre-strain (ε_{pre}). Hydrogen charging degraded TEl_f, irrespective of pre-strain. It should be noted that the pre-straining to 3–10% reduced the degree of hydrogen-induced degradation of the TEl_f when the specimens were charged with hydrogen at 1 A/m^2. The specimens charged with hydrogen at 10 A/m^2 also exhibited a similar trend in the pre-strain range of 6–10%. A factor that triggered the pre-strain effect can be a decrease in volume fraction of retained austenite via pre-deformation-induced martensitic transformation as shown in Fig. 2. The martensitic transformation during pre-straining avoided hydrogen supersaturation in the fresh martensite that occurred when hydrogen-charged austenite transformed to martensite (Hojo et al. 2019; Koyama et al. 2019). Additionally, the martensitic transformation during pre-straining decreased the probability of austenite/bainitic ferrite interface that acted as both preferential hydrogen localization site (Chan et al. 1991) and cracking site. Conversely, the advantageous effect of pre-strain on TEl_f disappeared when the pre-strain exceeded 12%. To explain the disappearance of the advantageous pre-strain effect, we here note that the pre-strained specimens showed higher yield strength than that of the specimen without pre-strain, due to work hardening (Fig. 4). Hydrogen-related cracking can be assisted by the work hardening associated with dislocation multiplication, deformation-induced martensitic transformation and pile-up of dislocations at lath, packet, block and prior austenite boundaries. The dislocation multiplication increased weak hydrogen trap site density (Choo and Lee 1982), thereby increasing diffusible hydrogen con-

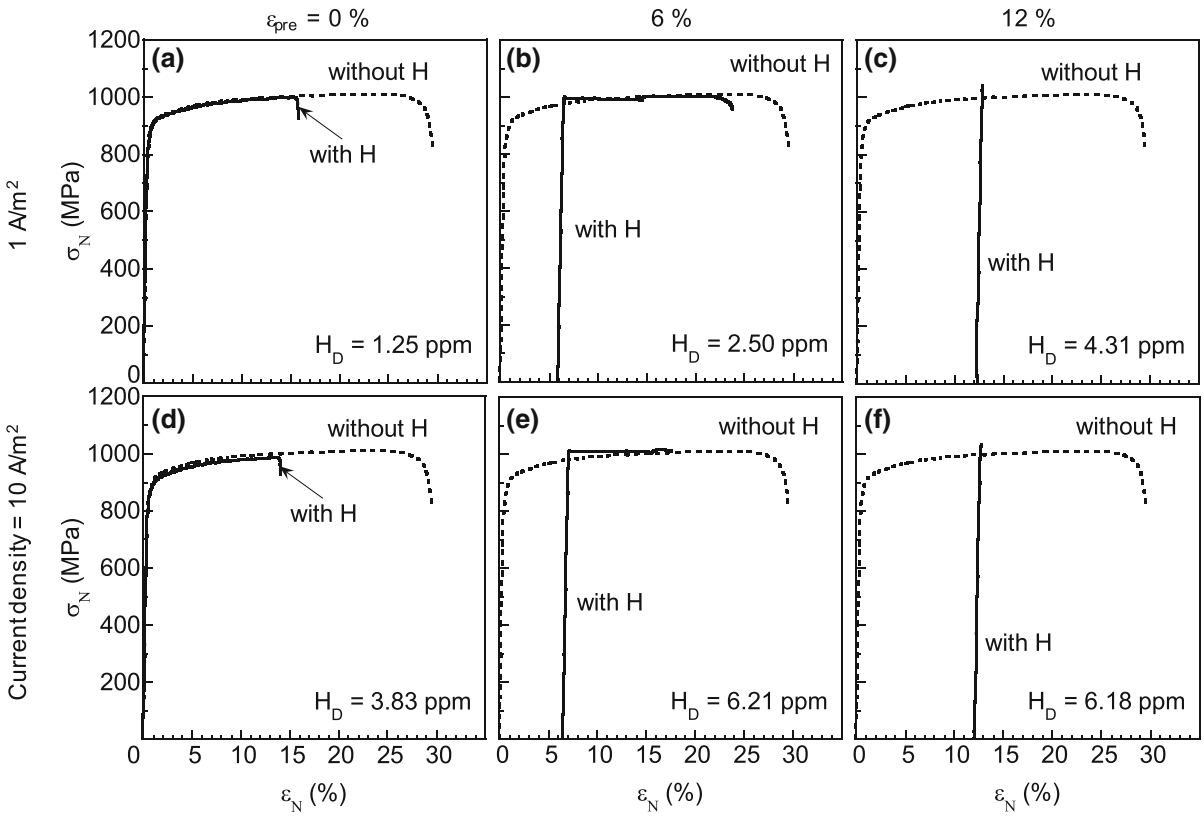

Fig. 4 Nominal stress (σ_N)–nominal strain (ε_N) curves of TBF steel pre-strained by (**a**, **d**) 0, (**b**, **e**) 6 and (**c**, **f**) 12% with hydrogen charging at current densities corresponding to (**a**–**c**) 1 and (**d**–**f**) 10 A/m^2. Hydrogen contents in the hydrogen charged specimens as measured after fracture are shown in the lower right

tent after pre-straining and subsequent hydrogen charging as shown in Fig. 4. When the number of dislocations interacting with hydrogen increases, hydrogen accumulation at martensite boundaries or dislocation arrays can be promoted by dislocation motion and subsequent pile-up, which assists boundary cracking or quasi-cleavage fracture (Nagao et al. 2012). These dislocation-driven phenomena potentially increased hydrogen embrittlement susceptibility when the properties were compared at an identical current density.

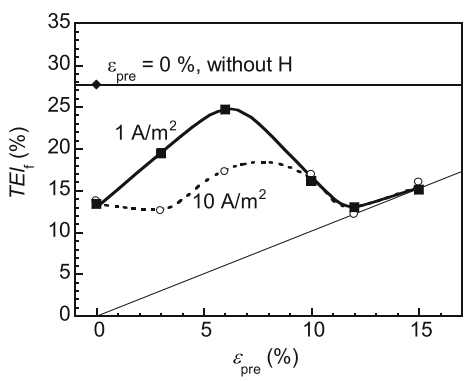

Fig. 5 Variations in total elongation (TEl_f) as a function of pre-strain (ε_{pre}), in which TEl_f is defined as the sum of elongations during pre-straining (ε_{pre}) and after hydrogen charging (ε_m), ($TEl_f = \varepsilon_{pre} + \varepsilon_m$)

3.3 Behavior of hydrogen-assisted fracture

The fracture surface of the TBF steel without hydrogen charging was fully covered with dimples (Fig. 6). Conversely, the fracture surface of the pre-strained and hydrogen charged specimens also exhibited dimples although their sizes exceeded that without hydrogen charging. Furthermore, the dimple size increased due to increases in the current density from 1 to 10 A/m^2

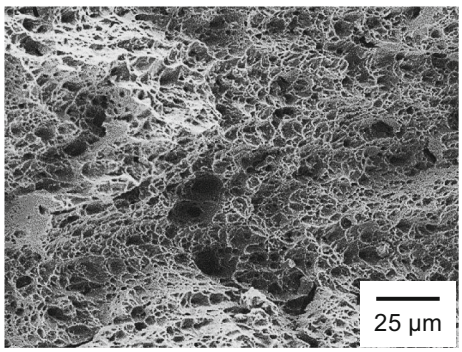

Fig. 6 Fracture surface of the specimen without pre-straining and hydrogen charging

as shown in Fig. 7. Generally, a dimple size of hydrogenated steels is reported as smaller than that without hydrogen (Marchi et al. 2008) although the present result revealed an opposite trend. To interpret the fracture behavior, microstructural cracking behavior constitutes a key as discussed below.

Figure 8 shows surface of the stretched part of tensile specimens after 6% straining without and with pre-hydrogen-charging at a current density of 1 A/m^2. Hydrogen charging was conducted before 6% straining. Evidently, the pre-hydrogen-charging increased probability of deformation-induced cracks on the specimen surface. It was reported that hydrogen-assisted cracking occurred at transformed martensite itself and/or matrix/transformed martensite interfaces and that resultant fracture occurred in multi-phase TRIP-aided steels (Laureys et al. 2016; Ronevich et al. 2012; Wang et al. 2015). Thus, it is expected that the hydrogen-charged TBF steel fractured in an early stage of the tensile test given that crack initiation and propagation at matrix/martensite interfaces were accelerated by the existence of transformed martensite in the TBF steel with hydrogen in a manner similar to that in previous studies (Hojo et al. 2018; Ronevich et al. 2012; Zhu et al. 2016). An important aspect of the observation in Fig. 8 corresponds to the presence of "multiple" cracks, which indicated that crack propagation once stopped (otherwise, the first crack initiation causes fracture without second crack initiation). This indicated that the crack coalescence process can act as a significant factor that causes the final failure of the hydrogen-charged TBF steel. In this context, crack initiation probability was also a crucial factor that affected crack growth via coalescence. Specifically, when a subcrack or potential crack initiation site (i.e., retained austenite in this case) exists in front of the main crack, the crack growth can be accelerated. Thus, the pre-strain effect that reduced fraction of retained austen-

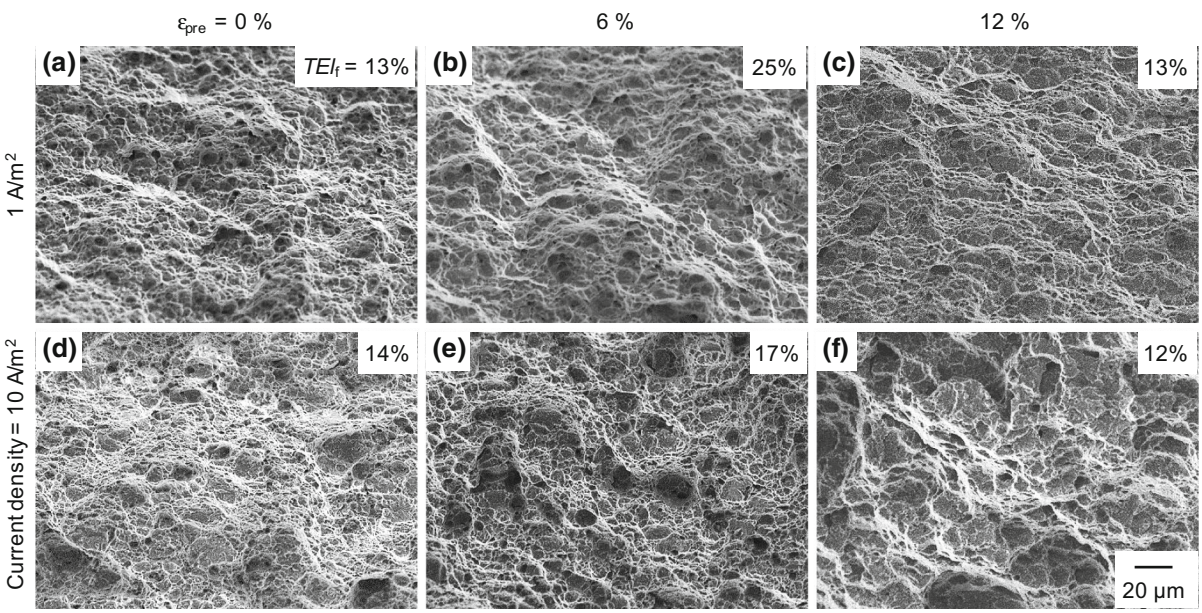

Fig. 7 Fracture surfaces of the specimens pre-strained to (**a**, **d**) 0%, (**b**, **e**) 6% and (**c**, **f**) 12% with hydrogen charging at current densities of (**a**–**c**) 1 and (**d**–**f**) 10 A/m^2

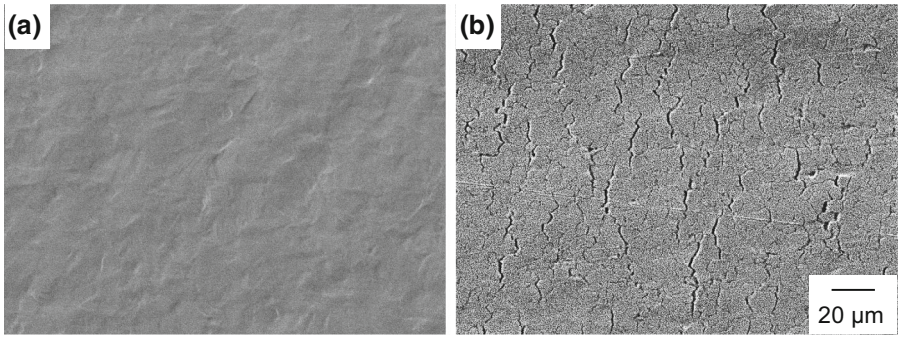

Fig. 8 Specimen surfaces of the gauge section with strain of 6% **a** without and **b** with hydrogen charging

ite directly contributed to resisting hydrogen-related crack growth because the martensite transformed from austenite acted as the preferential crack initiation site in the presence of hydrogen as previously mentioned. Additionally, it should be noted that the coarse dimple size shown in Fig. 7 was approximately 14 μm, which was significantly larger than the average dimple size of the uncharged specimen (3 μm). Also, the coarse dimple size was three times larger than the size of retained austenite before the test (shown in Fig. 1). These facts implied that the coarse dimples arose from the coalescence of a few cracks that formed from martensite transformed from retained austenite. This also supported the importance of pre-strain effect, which reduced crack initiation probability on resistance to the hydrogen-assisted fracture.

4 Conclusions

In the study, the tensile properties of pre-strained and hydrogen-charged TBF steel were investigated to evaluate the hydrogen embrittlement resistance of press-formed TBF steel. The main results are shown as follows.

(1) The total elongation at fracture of the TBF steel decreased by hydrogen charging when the pre-strain corresponded to 0–15%. The hydrogen-induced degradation of elongation appeared to be significant with increases in the hydrogen content.
(2) With respect to the total elongation at fracture, the 3–10% pre-straining improved the hydrogen embrittlement resistance when compared to that without pre-straining. However, the advantageous effect of pre-strain disappeared when the pre-strain was over 12%.
(3) The advantageous effect of pre-strain (3–10%) on hydrogen embrittlement resistance was attributed to the transformation of retained austenite prior to hydrogen charging, which suppressed crack initiation and propagation.
(4) The disappearance of the advantageous pre-strain effect at 12–15% pre-strain is potentially caused by the increase in the absorbed hydrogen due to pre-straining.

Acknowledgements The study was supported by JSPS KAKENHI Grant-in-Aid for Scientific Research on Innovative Areas "Hydrogenomics", Nos. JP18H05513 and JP18H05514 and Grant-in-Aid for Scientific Research (C), No. JP18K04743. Furthermore, the part of the study was financially supported by the Amada Foundation. Additionally, a part of this work was supported by the QST Advanced Characterization Nanotechnology Platform under the remit of "Nanotechnology Platform" of the Ministry of Education, Culture, Sports, Science and Technology (MEXT), Japan (Proposal Nos. A-17-QS-0024 and A-18-QS-0034). The synchrotron radiation experiments were performed using a QST experimental station at QST (JAEA) beamline BL14B1, SPring-8, with the approval of the Japan Synchrotron Radiation Research Institute (JASRI) (Proposal Nos. 2017B3681 and 2018B3681).

References

Caballero FG, GarcÍa-Mateo C, Chao J, Santofimia MJ, Capdevila C, AndrÉs CGD (2008) Effects of morphology and stability of retained austenite on the ductility of TRIP-aided bainitic steels. ISIJ Int 48:1256–1262. https://doi.org/10.2355/isijinternational.48.1256

Caballero FG, Roelofs H, Hasler S, Capdevila C, Chao J, Cornide J, Garcia-Mateo C (2013) Influence of bainite morphology on impact toughness of continuously cooled cementite free bainitic steels. Mater Sci Technol 28:95–102. https://doi.org/10.1179/1743284710Y.0000000047

Chan SLI, Lee HL, Yang JR (1991) Effect of retained austenite on the hydrogen content and effective diffusivity of martensitic structure. Metall Trans A 22A:2579–2586. https://doi.org/10.1007/BF02851351

Choo WY, Lee JY (1982) Thermal analysis of trapped hydrogen in pure iron. Metall Mater Trans A 13A:135–140. https://doi.org/10.1007/BF02642424

Dyson DJ, Holmes B (1970) Effect of alloying additions on the lattice parameter of austenite. J Iron Steel Inst 208:469–474

Hojo T, Sugimoto K-I, Mukai Y, Ikeda S (2008) Effects of aluminum on delayed fracture properties of ultra high strength low alloy TRIP-aided steels. ISIJ Int 48:824–829. https://doi.org/10.2355/isijinternational.48.824

Hojo T, Kobayashi J, Sugimoto K (2016) Impact properties of low-alloy transformation-induced plasticity-steels with different matrix. Mater Sci Technol 32:1035–1042. https://doi.org/10.1080/02670836.2015.1110665

Hojo T, Ukai Y, Akiyama E (2017) Effects of hydrogen on tensile properties at slow strain rate of ultra high-strength TRIP-aided bainitic ferrite steels. Procedia Eng 207:1868–1873. https://doi.org/10.1016/j.proeng.2017.10.953

Hojo T, Kikuchi R, Waki H, Nishimura F, Ukai Y, Akiyama E (2018) Effect of strain rate on the hydrogen embrittlement property of ultra high-strength low alloy TRIP-aided steel. ISIJ Int 58:751–759. https://doi.org/10.2355/isijinternational.ISIJINT-2017-576

Hojo T, Koyama M, Terao N, Tsuzaki K, Akiyama E (2019) Transformation-assisted hydrogen desorption during deformation in steels: examples of α' - and ε-martensite. Int J Hydrog Energy 44:30472–30477. https://doi.org/10.1016/j.ijhydene.2019.09.171

Koyama M, Yamasaki D, Ikeda A, Hojo T, Akiyama E, Takai K, Tsuzaki K (2019) Detection of hydrogen effusion before, during, and after martensitic transformation: example of multiphase transformation-induced plasticity steel. Int J Hydrog Energy 44:26028–26035. https://doi.org/10.1016/j.ijhydene.2019.07.254

Laureys A, Depover T, Petrov R, Verbeken K (2016) Microstructural characterization of hydrogen induced cracking in TRIP-assisted steel by EBSD. Mater Charact 112:169–179. https://doi.org/10.1016/j.matchar.2015.12.017

Marchi CS, Somerday BP, Tang X, Schiroky GH (2008) Effects of alloy composition and strain hardening on tensile fracture of hydrogen-precharged type 316 stainless steels. Int J Hydrog Energy 33:889–904. https://doi.org/10.1016/j.ijhydene.2007.10.046

Nagao A, Smith CD, Dadfarnia M, Sofronis P, Robertson IM (2012) The role of hydrogen in hydrogen embrittlement fracture of lath martensitic steel. Acta Materialia 60:5182–5189. https://doi.org/10.1016/j.actamat.2012.06.040

Peet MJ, Hojo T (2016) Hydrogen susceptibility of nanostructured bainitic steels. Metall Mater Trans A 47A:718–725. https://doi.org/10.1007/s11661-015-3221-9

Ronevich JA, Cooman BCD, Speer JG, Moor ED, Matlock DK (2012) Hydrogen effects in prestrained transformation induced plasticity steel. Metall Mater Trans A 43A:2293–2301. https://doi.org/10.1007/s11661-011-1075-3

Senuma T, Takemoto Y (2010) Influence of thermal history on microstructure and mechanical properties of steels for hot stamping. Mater Sci Forum 654–656:330–333. https://doi.org/10.4028/www.scientific.net/MSF.654-656.330

Song S-M, Sugimoto K-I, Kandaka S, Futamura A, Kobayashi M, Masuda S (2003) Effects of prestraining on high-cycle fatigue strength of high-strength low alloy TRIP-aided steels. Mater Sci Res Int 52:223–229. https://doi.org/10.2472/jsms.52.9Appendix_223

Sugimoto K-I, Nakano K, Song S-M, Kashima T (2002) Retained austenite characteristics and stretch-flangeability of high-strength low-alloy TRIP type bainitic sheet steels. ISIJ Int 42:450–455. https://doi.org/10.2355/isijinternational.42.450

Sugimoto K, Tsunezawa M, Hojo T, Ikeda S (2004) Ductility of 0.1-0.6C-1.5Si-1.5Mn ultra high-strength TRIP-aided sheet steels with bainitic ferrite matrix. ISIJ Int 44:1608–1614. https://doi.org/10.2355/isijinternational.44.1608

Takagi S, Toji Y, Yoshino M, Hasegawa K (2012) Hydrogen embrittlement resistance evaluation of ultra high strength steel sheets for automobiles. ISIJ Int 52:316–322. https://doi.org/10.2355/isijinternational.52.316

Takagi S, Hagihara Y, Hojo T, Urushihara W, Kawasaki K (2016) Comparison of hydrogen embrittlement resistance of high strength steel sheets evaluated by several methods. ISIJ Int 56:685–692. https://doi.org/10.2355/isijinternational.ISIJINT-2015-566

Tamura I (1970) Steel material study on the strength. Nikkan-Kogyo Shinbun Ltd., Tokyo

Wang M, Tasan CC, Koyama M, Ponge D, Raabe D (2015) Enhancing hydrogen embrittlement resistance of lath martensite by introducing nano-films of interlath austenite. Metall Mater Trans A 46A:3793–3802. https://doi.org/10.1007/s11661-015-3009-y

Yoshikawa N, Kobayashi J, Sugimoto K-I (2012) Notch-fatigue properties of advanced TRIP-aided bainitic ferrite steels. Metall Mater Trans A 43A:4129–4136. https://doi.org/10.1007/s11661-012-1246-x

Zackay VF, Parker ER, Fahr D, Bush R (1967) The enhancement of ductility in high-strength steels. Trans Am Soc Met 60:252–259

Zhou J, Wang B, Huang M-D, Cui D (2014) Effect of hot stamping parameters on the mechanical properties and microstructure of cold-rolled 22MnB5 steel strips. Int J Miner Metall Mater 21:544–555. https://doi.org/10.1007/s12613-014-0940-7

Zhu X, Zhang K, Li W, Jin X (2016) Effect of retained austenite stability and morphology on the hydrogen embrittlement susceptibility in quenching and partitioning treated steels. Mater Sci Eng A 658:400–408. https://doi.org/10.1016/j.msea.2016.02.026